

Nucleation through a Double Barrier on a Chemically Patterned Substrate

Antonio Valencia* and Reinhard Lipowsky†

Max-Planck-Institute of Colloids and Interfaces, D-14424 Potsdam, Germany

Received August 12, 2003. In Final Form: October 31, 2003

We study nucleation of liquid droplets from a one-component vapor phase on a planar lyophobic substrate, δ , patterned with a number of lyophilic (easily wettable) circular domains, γ . The wettabilities of the lyophilic domains and the lyophobic substrate are characterized by contact angles θ_γ and θ_δ , respectively. Depending on the supersaturation of the vapor and on the contact angles θ_γ and θ_δ , nucleation of a droplet on one of these circular domains proceeds through a free energy barrier with one or two maxima (a double barrier). Barriers with two maxima occur for *intermediate* values of the supersaturation. In terms of the dimensionless supersaturation Δ , this intermediate regime is given by $\sin \theta_\gamma < \Delta < \sin \theta_\delta$ for $\theta_\gamma < \theta_\delta < \pi/2$ and by $\sin \theta_\gamma < \Delta < 1$ for $\theta_\gamma < \pi/2 < \theta_\delta$. We extend classical nucleation theory to account for the kinetics of nucleation through a double barrier and apply this extension to the nucleation of droplets on lyophilic circular domains.

1. Introduction

In recent years, experimental techniques have been developed that allow the patterning of a substrate with different types of surface domains, which have a molecular thickness and an area in the mesoscopic scale and which exhibit different wettabilities.^{1–7} For example, domain sizes of 30 nm have been created using an atomic force microscope, the “tip” of which was brought into contact with a flat surface.⁸

The existence of new patterned surfaces has led to increased theoretical efforts to understand wetting phenomena in such systems; see refs 9–16 and the review in ref 17. These efforts have been mainly concerned with the equilibrium morphologies of wetting layers and droplets on chemically patterned substrates. In particular, mor-

phological wetting transitions, that is, transitions in the shapes of the wetting layers when the volume of liquid is changed, have been discovered and studied for several types and patterns of surface domains.^{11,13,16,17}

In this article, we address the question of how morphological wetting transitions affect the kinetics of the vapor–liquid phase transition. In particular, we study the kinetics of the condensation of droplets from a one-component vapor phase on a lyophobic substrate patterned with a number of lyophilic (easily wettable) circular domains.

It was first pointed out by Gibbs that the metastability of a vapor phase depends on the energy necessary to form a critical nucleus, that is, a droplet of a certain critical size.¹⁸ Droplets smaller than this critical size tend to disappear, while droplets larger than the critical size tend to grow. The corresponding excess free energy has an activation barrier with its maximum at the critical size. Classical nucleation theory describes droplet nucleation and growth as a thermally activated process over this free energy barrier.^{19–24} This applies both to droplets that are formed in the bulk of the vapor phase (homogeneous nucleation) and to those that grow at a chemically uniform wall (heterogeneous nucleation).

The problem of finding the activation barrier for the condensation of a droplet on a single lyophilic surface domain has been studied theoretically.^{25,26} It was shown that the condensation of a droplet on a lyophilic circular domain proceeds through a barrier with one or two maxima (a double barrier). In the present article, we will show that free energy barriers with two maxima occur for *intermediate* values of the supersaturation. In terms of the dimensionless supersaturation Δ , this intermediate regime is given by $\sin \theta_\gamma < \Delta < \sin \theta_\delta$ for $\theta_\gamma < \theta_\delta < \pi/2$

* Author to whom correspondence should be addressed. E-mail: valencia@mpimp-golm.mpg.de. Current address: Max Planck Institute of Molecular Plant Physiology, 14424 Potsdam, Germany.

† URL: <http://www.mpikg-golm.mpg.de/lipowsky>.

(1) Drelich, J.; Miller, J. D.; Kumar, A.; Whitesides, G. M. *Colloids Surf., A* **1994**, *93*, 1–13.

(2) Morhard, F.; Schumacher, J.; Lenenbach, A.; Wilhelm, T.; Dahint, R.; Grunze, M.; Everhart, D. S. *Electrochem. Soc. Proc.* **1997**, *97*, 1058–1063.

(3) Herminghaus, S.; Fery, A.; Reim, D. *Ultramicroscopy* **1997**, *69*, 211–217.

(4) Burmeister, F.; Schäfle, C.; Matthes, T.; Böhmisch, M.; Boneberg, J.; Leiderer, P. *Langmuir* **1997**, *13*, 2983–2987.

(5) Drodofsky, U.; Stuhler, J.; Schulze, T.; Drewsen, M.; Brezger, B.; Pfau, T.; Mlynek, J. *Appl. Phys. B* **1997**, *65*, 755–759.

(6) Heier, J.; Kramer, E. J.; Walheim, S.; Krausch, G. *Macromolecules* **1997**, *30*, 6610–6614.

(7) Möller, G.; Harke, M.; Motschmann, H. *Langmuir* **1998**, *14*, 4955.

(8) García, R.; Calleja, M.; Pérez-Murano, F. *Appl. Phys. Lett.* **1998**, *72*, 2295–2297.

(9) Röcken, P.; Tarazona, P. *J. Chem. Phys.* **1996**, *105*, 2034–2043.

(10) Schoen, M.; Diestler, D. *J. Chem. Phys. Lett.* **1997**, *270*, 339–344.

(11) Lenz, P.; Lipowsky, R. *Phys. Rev. Lett.* **1998**, *80*, 1920.

(12) Röcken, P.; Somoza, A.; Tarazona, P.; Findenegg, G. *J. Chem. Phys.* **1998**, *108*, 8689–8697.

(13) Gau, H.; Herminghaus, S.; Lenz, P.; Lipowsky, R. *Science* **1999**, *283*, 46–49.

(14) Bock, H.; Schoen, M. *Phys. Rev. E* **1999**, *59*, 4122–4136.

(15) Bauer, C.; Dietrich, S.; Parry, A. O. *Europhys. Lett.* **1999**, *47*, 474–480.

(16) Valencia, A.; Brinkmann, M.; Lipowsky, R. *Langmuir* **2001**, *17*, 3390–3399.

(17) Lipowsky, R. *Curr. Opin. Colloid Interface Sci.* **2001**, *6*, 40–48.

(18) *The scientific papers of J. Willard Gibbs*; Dover: New York, 1961.

(19) Volmer, M.; Weber, A. *Z. Phys. Chem.* **1926**, *119*, 277–301.

(20) Farkas, L. *Z. Phys. Chem.* **1927**, *125*, 236–242.

(21) Becker, R.; Döring, W. *Ann. Phys.* **1935**, *24*, 719.

(22) Volmer, M. *Kinetik der Phasenbildung*; Verlag von Theodor Steinkopf: Dresden und Leipzig, 1939.

(23) Frenkel, J. *J. Chem. Phys.* **1939**, *7*, 538–547.

(24) Frenkel, J. *Kinetic theory of liquids*; Dover: New York, 1955.

(25) Smorodin, V. E. *Sov. Phys. Dokl.* **1987**, *32*, 405–407.

(26) Smorodin, V. E. *Langmuir* **1994**, *10*, 2250–2256.

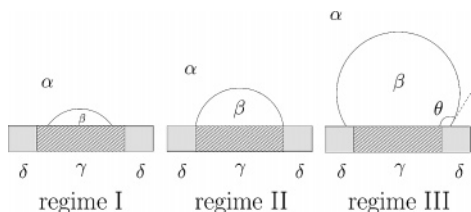


Figure 1. Three different regimes for a spherical droplet located on a lyophilic circular domain. The *actual* contact angle θ of the droplet is equal to θ_γ in regime I and θ_δ in regime III, but satisfies $\theta_\gamma \leq \theta \leq \theta_\delta$ in regime II.

and by $\sin \theta_\gamma < \Delta < 1$ for $\theta_\gamma < \pi/2 < \theta_\delta$, where θ_γ and θ_δ are the contact angles of the liquid with the lyophilic and lyophobic surface domains, respectively. In addition, we extend classical nucleation theory and address the kinetics of nucleation through such double barriers.

Our article is organized as follows. In section 2, we study the barrier for the nucleation of a droplet on a lyophilic circular domain. In section 3, we derive the equilibrium cluster size distribution for the droplets condensed from a vapor phase in contact with a substrate patterned with a number of lyophilic circular domains. Section 4 is devoted to the fundamental equations of the kinetic model used in classical nucleation theory. In section 5, we solve the problem of the nucleation through a double barrier in the steady state. Finally, section 6 summarizes the most relevant results.

2. Droplets on a Lyophilic Circular Domain

2.1. Three Regimes for Equilibrium Droplets. Let us consider a certain amount of condensed liquid phase β that is in contact with its vapor α and with a planar substrate σ . Most of the surface of the substrate consists of a lyophobic phase δ , but it also contains a lyophilic γ domain. The latter surface domain is taken to be circular with radius r_γ . The contact angles on the lyophilic and on the lyophobic surface regions are θ_γ and θ_δ , respectively, with $\theta_\gamma < \theta_\delta$. The substrate is rigid, and its composition does not change during the wetting processes.

In this subsection, the droplet is in a stable state that is characterized by a constant volume of liquid V_β and mechanical equilibrium of the interface between the vapor α and the liquid β . Such a situation may correspond to a liquid, which is nonvolatile on the experimentally relevant time scales. In this case, the state of lowest free energy corresponds to a droplet that forms a spherical cap and that is in contact with the lyophilic γ domain.

In general, the β droplet on the σ substrate is bounded by two interfaces: the α - β interface with area $A_{\alpha\beta}$, and the β - σ interface with area $A_{\beta\sigma}$. Its interfacial free energy is then given by

$$\Delta F = A_{\alpha\beta}\Sigma_{\alpha\beta} + A_{\beta\sigma}(\Sigma_{\beta\sigma} - \Sigma_{\alpha\sigma}) \quad (1)$$

with the corresponding interfacial tensions Σ_{ij} . The spherical cap is obtained if one minimizes this free energy under the constraint of fixed volume V_β . In fact, this minimization leads to three different droplet regimes as shown in Figure 1.^{11,25}

The simplest way to characterize these different droplet regimes is via the location of the contact line of the droplet. In regime I, the contact line is located within the lyophilic γ domain and the contact angle is $\theta = \theta_\gamma$. Likewise, regime III is characterized by a contact line on the lyophobic surface region with $\theta = \theta_\delta$. Finally, in regime

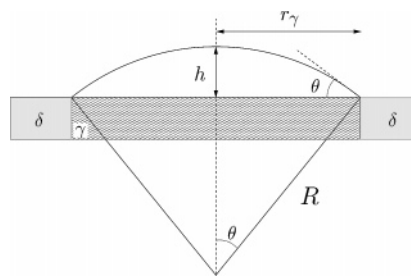


Figure 2. Geometry of a droplet that completely covers a circular γ domain of radius r_γ (regime II). The droplet forms a spherical cap with curvature radius R , contact angle θ , and height h .

II, the contact line is on top of the γ - δ domain boundary and the contact angle θ can attain any value within the range $\theta_\gamma \leq \theta \leq \theta_\delta$.

To characterize these regimes in more detail, it is useful to recall some elementary features of spherical caps. These caps have a constant curvature radius that we will denote by R . Their volume is given by

$$V_\beta = \Phi(\theta)^4/3\pi R^3 \quad (2)$$

with

$$\Phi(\theta) \equiv 1/4(1 - \cos \theta)^2(2 + \cos \theta) \quad (3)$$

which is equal to the ratio between the actual volume of the droplet and the volume of a complete sphere with equal curvature radius.

The three droplet regimes can now be defined by the two boundary volumes

$$V_1 \equiv \Phi(\theta_\gamma)^4/3\pi R_1^3 \quad \text{with} \quad R_1 \equiv r_\gamma/\sin \theta_\gamma \quad (4)$$

and

$$V_2 \equiv \Phi(\theta_\delta)^4/3\pi R_2^3 \quad \text{with} \quad R_2 \equiv r_\gamma/\sin \theta_\delta \quad (5)$$

The two droplets with volumes $V_\beta = V_1$ and $V_\beta = V_2$ have the same contact area $A_\gamma \equiv \pi r_\gamma^2$, which is the area of the lyophilic γ domain, but differ in their contact angles, which are $\theta = \theta_\gamma$ and $\theta = \theta_\delta$, respectively.

These two boundary volumes define three intervals: $0 < V_\beta < V_1$, which corresponds to regime I; the intermediate volume range $V_1 \leq V_\beta \leq V_2$ corresponding to regime II; and $V_2 < V_\beta$, which defines regime III. Thus, the volumes V_1 and V_2 correspond to the smallest and the largest droplets in regime II, respectively.

The two interfaces bounding the spherical cap of radius R have the areas $A_{\alpha\beta} = 2\pi R^2(1 - \cos \theta)$ and $A_{\beta\sigma} = \pi R^2 \sin^2 \theta$. The latter area is smaller than the area $A_\gamma = \pi r_\gamma^2$ of the lyophilic γ domain in regime I, is equal to A_γ in regime II, and exceeds this area in regime III.

Another geometric quantity that can be used to uniquely define the three droplet regimes is the height h of the spherical cap, which is given by

$$h = R(1 - \cos \theta) \quad (6)$$

and increases monotonically with increasing V_β ; see Figure 2.

In regime II, the radius of curvature R is related to the contact angle θ by $R = r_\gamma/\sin \theta$, and the area $A_{\alpha\beta}$ and the volume V_β are related to the height h of

the spherical cap by the expressions $A_{\alpha\beta} = \pi(h^2 + r_\gamma^2)$ and $V_\beta = \pi h(h^2 + 3r_\gamma^2)/6$, respectively.

Using these relations, one may now calculate the interfacial free energy as given by eq 1, which leads to the relations

$$\Delta F = \Delta F_I \equiv \sum_{\alpha\beta} \Phi(\theta_\gamma) 4\pi R^2 \quad (7)$$

for regime I,

$$\Delta F = \Delta F_{II} \equiv \sum_{\alpha\beta} \pi [h^2 + r_\gamma^2 (1 - \cos \theta_\gamma)] \quad (8)$$

for regime II, and

$$\Delta F = \Delta F_{III} \equiv \sum_{\alpha\beta} [\Phi(\theta_\delta) 4\pi R^2 - \pi r_\gamma^2 (\cos \theta_\gamma - \cos \theta_\delta)] \quad (9)$$

for regime III. These three equations also define the interfacial free energy ΔF as a function of the droplet volume V_β . With the use of the implicit function theorem, it is not difficult to show that both ΔF and the first derivative $\partial\Delta F/\partial V_\beta$ are continuous at the boundary volumes V_1 and V_2 even though various functions such as, for example, $\partial R/\partial V_\beta$, are not continuous at these points.

2.2. Droplets in Contact with a Supersaturated Vapor. We will now move our system out of equilibrium and consider a situation in which the vapor α is supersaturated and, thus, in a metastable bulk state. In classical nucleation theory, one determines the minimal work necessary to form a droplet when the fluid is in contact with a thermal reservoir at temperature T and with a work reservoir at pressure $P = P_\alpha$.²⁷ If the droplet contains N_β molecules, this minimal work or excess free energy has the general form

$$\Delta G = \Delta F + (P_\alpha - P_\beta) V_\beta + N_\beta [\mu_\beta(T, P_\beta) - \mu_\alpha(T, P_\alpha)] \quad (10)$$

with the interfacial free energy ΔF as given by eqs 7–9.

We will now ignore the compressibility of the liquid and take its particle number density to be constant and equal to ρ_β . Integration of the relation $(\partial\mu_\beta/\partial P)_T = 1/\rho_\beta$, which follows from the Gibbs–Duhem equation at a constant temperature, then leads to

$$\mu_\beta(T, P_\beta) - \mu_\beta(T, P_\alpha) = (P_\beta - P_\alpha)/\rho_\beta \quad (11)$$

If we insert this relation into eq 10, the excess free energy attains the simpler form

$$\Delta G = \Delta F - \Delta\mu\rho_\beta V_\beta \quad (12)$$

which depends on the supersaturation

$$\Delta\mu \equiv \Delta\mu(T, P_\alpha) \equiv \mu_\alpha(T, P_\alpha) - \mu_\beta(T, P_\alpha) \quad (13)$$

where $\mu_\alpha(T, P_\alpha)$ and $\mu_\beta(T, P_\alpha)$ are the chemical potentials in the vapor phase α and the liquid droplet β , both taken at the vapor pressure P_α .

Stationary droplet states correspond to those volumes for which

$$\partial\Delta G/\partial V_\beta = \partial\Delta F/\partial V_\beta - \rho_\beta\Delta\mu = 0 \quad (14)$$

For the interfacial free energy ΔF as given by eqs 7–9, one finds after some algebra that

$$\partial\Delta F/\partial V_\beta = 2\sum_{\alpha\beta}/R \quad (15)$$

in all three regimes. When this is inserted into eq 14, one obtains the rather simple relation

$$R = R_* \equiv 2\sum_{\alpha\beta}/\rho_\beta\Delta\mu \quad (16)$$

It follows that any stationary droplet state is characterized by a curvature radius R that is equal to $R_* \sim 1/\Delta\mu$. Thus, we will call R_* the *stationary radius*.

Because the interface bounding a stationary droplet should be in mechanical equilibrium, the curvature radius R of the droplet should also obey the Laplace equation

$$P_\beta - P_\alpha = 2\sum_{\alpha\beta}/R \quad (17)$$

When inserted into eq 16, this latter relation leads to $\Delta\mu = (P_\beta - P_\alpha)/\rho_\beta$. Using the definition 13 of the supersaturation $\Delta\mu$ and the integrated Gibbs–Duhem eq 11, one then obtains the simple equality $\mu_\beta(T, P_\beta) = \mu_\alpha(T, P_\alpha)$ for the chemical potentials of the stationary droplet and the supersaturated vapor. Starting from this latter equality, we could have derived the relation 16 directly from the Laplace eq 17 and the integrated Gibbs–Duhem eq 11.

For a chemically patterned substrate as discussed here, one may have more than one stationary droplet state for a given supersaturation $\Delta\mu$. This is shown in the next subsection using a simple graphical method.

2.3. Stationary Droplet States. To determine the possible stationary droplet states, which are the states that satisfy the relation $R = R_*$, we will now discuss the functional dependence of the curvature radius R on the droplet volume V_β .

In regimes I and III, the contact angle is fixed and the curvature radius R increases monotonically with increasing volume V_β . In regime II, the situation is different because R may decrease or increase with increasing volume V_β in different ranges of V_β depending on the values of the contact angles θ_γ and θ_δ .

Let us define $V_{sp}/2 \equiv (2\pi/3)r_\gamma^3$, which corresponds to the volume of a half-sphere with radius r_γ . In general, the functional dependence of the curvature radius R on the volume V_β exhibits the following qualitative features:

(A) For $\theta_\gamma < \theta_\delta < \pi/2$, one has $V_1 < V_2 < V_{sp}/2$. In this case, the curvature radius R increases for small V_β with $0 < V_\beta < V_1$, decreases for intermediate V_β with $V_1 < V_\beta < V_2$, and increases again for $V_2 < V_\beta$. Therefore, the curvature radius $R = R(V_\beta)$ has a minimum at $V_\beta = V_2$, where it attains the value $R = R_2 = r_\gamma/\sin \theta_\delta$, see Figure 3A.

(B) For $\theta_\gamma < \pi/2 < \theta_\delta$, one has $V_1 < V_{sp}/2 < V_2$. The curvature radius R increases for small V_β with $0 < V_\beta < V_1$, decreases for intermediate V_β with $V_1 < V_\beta < V_{sp}/2$, and increases again for $V_{sp}/2 < V_\beta$. Thus, $R = R(V_\beta)$ exhibits a minimum at $V_\beta = V_{sp}/2$, where it attains the value $R = r_\gamma$; see parts B.1 and B.2 of Figure 3.

(C) For $\pi/2 < \theta_\gamma < \theta_\delta$, one has $V_{sp}/2 < V_1 < V_2$. The droplet never attains the shape of a half-sphere, and R increases monotonically with V_β in all three regimes; see Figure 3C.

Using these general features of the functional dependence of $R = R(V_\beta)$, we can now classify the possible solutions of $R(V_\beta) = R_* \sim 1/\Delta\mu$. First, we may distinguish cases A and B from case C: For the latter case, $\pi/2 < \theta_\gamma < \theta_\delta$, $R = R(V_\beta)$ increases monotonically for all values of

(27) Debenedetti, P. G. *Metastable Liquids*; Princeton University Press: Princeton, New Jersey, 1996.

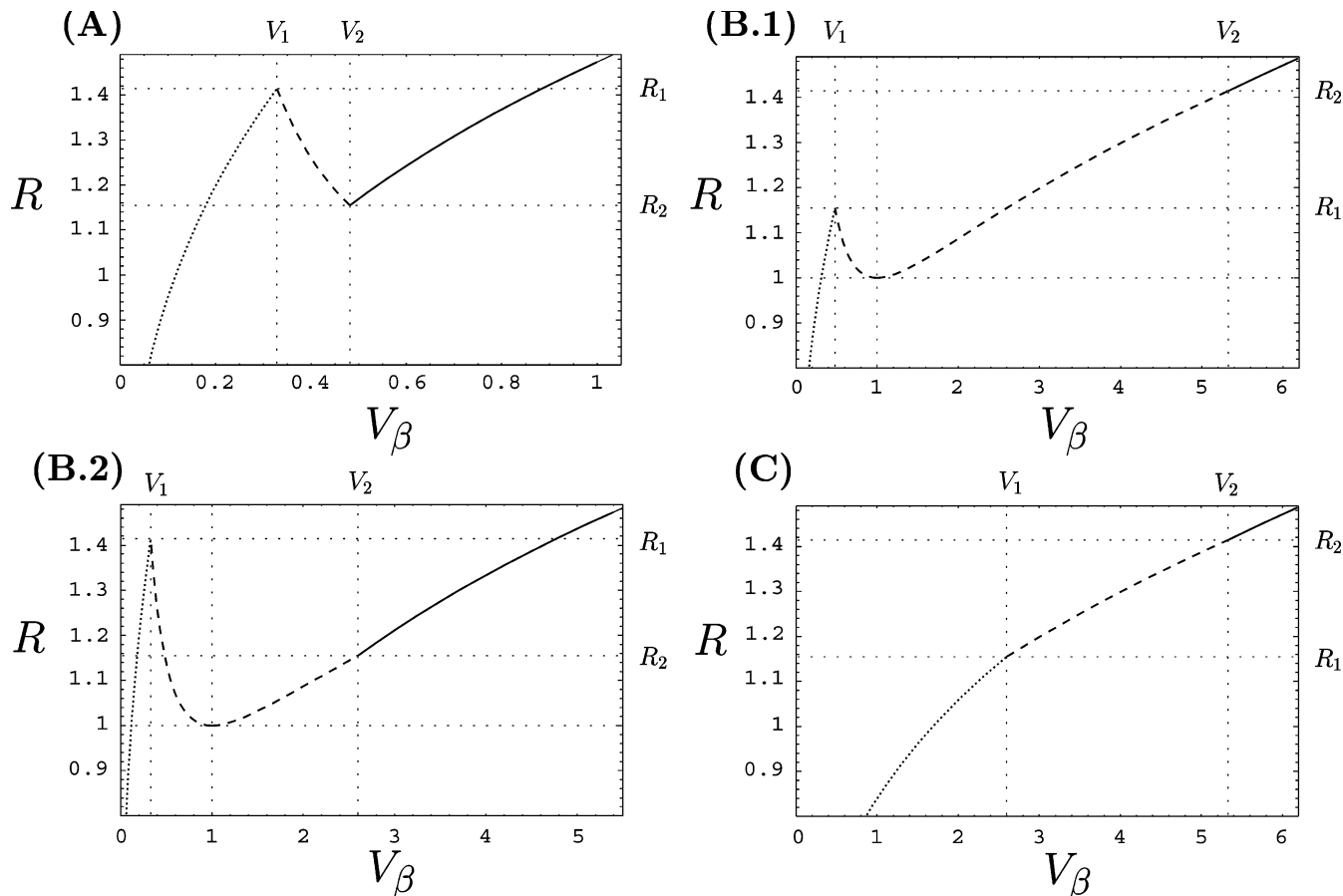


Figure 3. Functional dependence of curvature radius R on droplet volume V_β for the four different parameter regimes A, B.1, B.2, and C, as described in the text. The examples shown here correspond to the contact angles (A) $\theta_\gamma = \pi/4$ and $\theta_\delta = \pi/3$, (B.1) $\theta_\gamma = \pi/3$ and $\theta_\delta = 3\pi/4$, (B.2) $\theta_\gamma = \pi/4$ and $\theta_\delta = 2\pi/3$, and (C) $\theta_\gamma = 2\pi/3$ and $\theta_\delta = 3\pi/4$. The radii R , R_1 , and R_2 are given in units of the radius of the lyophilic circular domain r_γ . The volumes V_β , V_1 , and V_2 are given in units of the volume of the half-sphere of radius r_γ , which is given by $V_{sp}/2 \equiv (2\pi/3)r_\gamma^3$. In each case, the dotted curve corresponds to regime I, the dashed curve to regime II, and the solid curve to regime III.

V_β , and $R(V_\beta) = R_*$ always has a *single* solution; see Figure 3C. For $\theta_\gamma < \pi/2$, cases A and B, there is an intermediate range of R_* values for which $R(V_\beta) = R_*$ has *more than one* solution, as can be seen by inspection of parts A, B.1, and B.2 of Figure 3.

In case A, $\theta_\gamma < \theta_\delta < \pi/2$, the minimum of $R = R(V_\beta)$ corresponds to $R = R_2$, and one has more than one solution provided

$$R_2 \leq R_* \leq R_1 \quad (\text{for } \theta_\gamma < \theta_\delta < \pi/2) \quad (18)$$

More precisely, the equation $R(V_\beta) = R_*$ has two solutions both for $R_* = R_1$ and for $R_* = R_2$ and three solutions for $R_2 < R_* < R_1$.

In case B, $\theta_\gamma < \pi/2 < \theta_\delta$, the minimum of $R = R(V_\beta)$ corresponds to $R = r_\gamma$, and the condition to have more than one solution is

$$r_\gamma \leq R_* \leq R_1 \quad (\text{for } \theta_\gamma < \pi/2 < \theta_\delta) \quad (19)$$

Thus, the equation $R(V_\beta) = R_*$ has two solutions both for $R_* = R_1$ and for $R_* = r_\gamma$ and three solutions for $r_\gamma < R_* < R_1$.

The character of these solutions can be inferred from the general features of the excess free energy $\Delta G = \Delta G(V_\beta)$, as given by eq 12. This excess free energy vanishes for $V_\beta = 0$ and goes to minus infinity for large V_β . Therefore, whenever $R(V_\beta) = R_*$ has a single solution, this solution corresponds to a *maximum* of the excess free energy $\Delta G = \Delta G(V_\beta)$. Likewise, if this relation has three solutions, the small-volume and the large-volume solutions

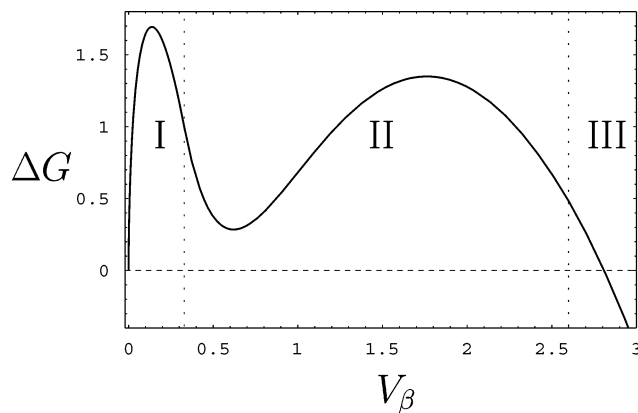


Figure 4. Excess free energy ΔG as a function of the droplet volume V_β for parameter regime B.2 with a double barrier. The contact angles are $\theta_\gamma = \pi/4$ and $\theta_\delta = 2\pi/3$. The stationary radius corresponding to the three extrema of $\Delta G = \Delta G(V_\beta)$ is R_* , $= 1.06r_\gamma$, where r_γ is the radius of the lyophilic domain. The volume V_β is given in units of the half-sphere volume as in Figure 3. The excess free energy ΔG is normalized to its value at $V_\beta = V_1$, where V_1 is the volume of the smallest droplet in regime II. The regions denoted by I, II, and III correspond to the regimes of a droplet on a lyophilic circular domain.

correspond to two maxima of $\Delta G = \Delta G(V_\beta)$, whereas the solution at intermediate V_β corresponds to a minimum. An example of the functional form of $\Delta G = \Delta G(V_\beta)$ showing two maxima is given in Figure 4. In the cases in which $R(V_\beta) = R_*$ has two solutions, one of them corresponds to

Table 1. Maxima and Minimum of $\Delta G = \Delta G(V_\beta)$ for Different Values of the Contact Angles, θ_γ and θ_δ , and of the Stationary Radius, $R_* \equiv 2\Sigma_{\alpha\beta}/\rho_\beta\Delta\mu^a$

R_*	Δ	regime I	regime II	regime III
		(A) $\theta_\gamma < \theta_\delta < \pi/2$		
$R_* < R_2$	$\sin \theta_\delta < \Delta$	1 max		
$R_2 < R_* < R_1$	$\sin \theta_\gamma < \Delta < \sin \theta_\delta$	1 max	1 min	1 max
$R_1 < R_*$	$\Delta < \sin \theta_\gamma$			1 max
		(B.1) $\theta_\gamma < \pi/2 < \theta_\delta$ and $\sin \theta_\delta < \sin \theta_\gamma$		
$R_* < r_\gamma$	$1 < \Delta$	1 max		
$r_\gamma < R_* < R_1$	$\sin \theta_\gamma < \Delta < 1$	1 max	1 min and 1 max	
$R_1 < R_* < R_2$	$\sin \theta_\delta < \Delta < \sin \theta_\gamma$		1 max	
$R_2 < R_*$	$\Delta < \sin \theta_\delta$			1 max
		(B.2) $\theta_\gamma < \pi/2 < \theta_\delta$ and $\sin \theta_\gamma < \sin \theta_\delta$		
$R_* < r_\gamma$	$1 < \Delta$	1 max		
$r_\gamma < R_* < R_2$	$\sin \theta_\delta < \Delta < 1$	1 max	1 min and 1 max	
$R_2 < R_* < R_1$	$\sin \theta_\gamma < \Delta < \sin \theta_\delta$	1 max	1 min	
$R_1 < R_*$	$\Delta < \sin \theta_\gamma$			1 max
		(C) $\pi/2 < \theta_\gamma < \theta_\delta$		
$R_* < R_1$	$\sin \theta_\gamma < \Delta$	1 max		
$R_1 < R_* < R_2$	$\sin \theta_\delta < \Delta < \sin \theta_\gamma$		1 max	
$R_2 < R_*$	$\Delta < \sin \theta_\delta$			1 max

^a The quantity $\Delta \equiv r_\gamma/R_*$ is the reduced supersaturation, where r_γ is the radius of the lyophilic circular domain. The radii R_1 and R_2 are $R_1 \equiv r_\gamma/\sin \theta_\gamma$ and $R_2 \equiv r_\gamma/\sin \theta_\delta$. The condition $\sin \theta_\delta < \sin \theta_\gamma$ is equivalent to $R_1 < R_2$, and $\sin \theta_\gamma < \sin \theta_\delta$ is equivalent to $R_2 < R_1$.

a maximum of $\Delta G = \Delta G(V_\beta)$ and the other one to a shoulder located either at the right or at the left of the maximum.

2.4. Different Nucleation Regimes. In a condensation experiment, one can change the stationary droplet radius R_* by varying the supersaturation $\Delta\mu$, which depends on the vapor pressure P_α . To determine the relation between these two quantities, let us briefly consider a planar α - β interface in equilibrium. In this case, the pressures in both phases are equal, that is, $P_\alpha = P_\beta \equiv P_0$. At a constant temperature, one has the Gibbs–Duhem relations $(\partial\mu_\alpha/\partial P)_T = 1/\rho_\alpha$ and $(\partial\mu_\beta/\partial P)_T = 1/\rho_\beta$, where ρ_α and ρ_β are the particle number densities in the vapor and in the liquid phases, respectively. Integrating these equations between P_0 and P_α , one obtains

$$\Delta\mu = \int_{P_0}^{P_\alpha} \left(\frac{1}{\rho_\alpha} - \frac{1}{\rho_\beta} \right) dP \approx T \ln(P_\alpha/P_0) \quad (20)$$

where we have assumed in the second (approximate) equality that $\rho_\alpha \ll \rho_\beta$ and that the vapor behaves as an ideal gas ($P_\alpha = \rho_\alpha T$, with the temperature T measured in energy units).

It is convenient to introduce the reduced supersaturation Δ via

$$\Delta \equiv r_\gamma/R_* = (\rho_\beta r_\gamma / 2\Sigma_{\alpha\beta}) \Delta\mu \approx (T\rho_\beta r_\gamma / 2\Sigma_{\alpha\beta}) \ln(P_\alpha/P_0) \quad (21)$$

In terms of this reduced supersaturation, the conditions for the existence of more than one stationary droplet state, eqs 18 and 19, become

$$\sin \theta_\gamma \leq \Delta \leq \sin \theta_\delta \quad \text{for} \quad \theta_\gamma < \theta_\delta < \pi/2 \quad (22)$$

and

$$\sin \theta_\gamma \leq \Delta \leq 1 \quad \text{for} \quad \theta_\gamma < \pi/2 < \theta_\delta \quad (23)$$

respectively.

In Table 1, we have classified the maxima and minimum of the activation barrier by the droplet regimes (I, II, or III) in which they occur, for different values of the reduced supersaturation $\Delta \sim 1/R_*$ and of the contact angles θ_γ and θ_δ . In Figure 5, we plot $\Delta G = \Delta G(R_*)$ in the stationary states [maxima and minimum of $\Delta G = \Delta G(V_\beta)$] for numerical examples of the cases detailed in Table 1.

For $\pi/2 < \theta_\gamma < \theta_\delta$, which corresponds to case C in Table 1, Figure 3, and Figure 5, there is only one stationary droplet for any value of the supersaturation $\Delta \sim \Delta\mu$. This stationary droplet corresponds to a single maximum of the excess free energy $\Delta G = \Delta G(V_\beta)$ and represents a single activation barrier for droplet nucleation. This is the same situation as that for droplet nucleation on a chemically uniform substrate.

For $\theta_\gamma < \pi/2$, which applies to cases A, B.1, and B.2 in Table 1, Figure 3, and Figure 5, on the other hand, we can distinguish three different nucleation regimes: For *small* supersaturations with $\Delta < \sin \theta_\gamma$, there is only one stationary droplet corresponding to a single barrier of the excess free energy $\Delta G = \Delta G(V_\beta)$. For *intermediate* supersaturations with $\sin \theta_\gamma < \Delta < \sin \theta_\delta$ in case A and $\sin \theta_\gamma < \Delta < 1$ in cases B.1 and B.2, one has a double barrier for nucleation. Hence, the excess free energy $\Delta G = \Delta G(V_\beta)$ exhibits two maxima separated by a minimum. The minimum corresponds to a droplet with contact angle

$$\theta = \arcsin \Delta = \arcsin(r_\gamma/R_*) < \pi/2 \quad (24)$$

Finally, for *large* supersaturations with $\sin \theta_\delta < \Delta$ in case A and $1 < \Delta$ in cases B.1 and B.2, one has again only one stationary droplet and, thus, a nucleation barrier with only one maximum.

3. Equilibrium and Zero-Flux Distributions of Droplet Sizes

Let us consider a lyophobic substrate patterned with N lyophilic circular domains in contact with a vapor phase at constant pressure P_α . We make the following assumptions:

(i) The nucleation of droplets only occurs on the lyophilic domains. The nucleation on the lyophobic surface or directly in the bulk of the vapor phase is very unlikely in comparison with the nucleation on the lyophilic domains. Alternatively, one may assume that the nucleation on the lyophobic surface and in the bulk of the vapor phase does occur but has no effect on the condensation on the lyophilic domains.

(ii) Neighboring lyophilic domains are located sufficiently far apart so that the droplets do not exchange

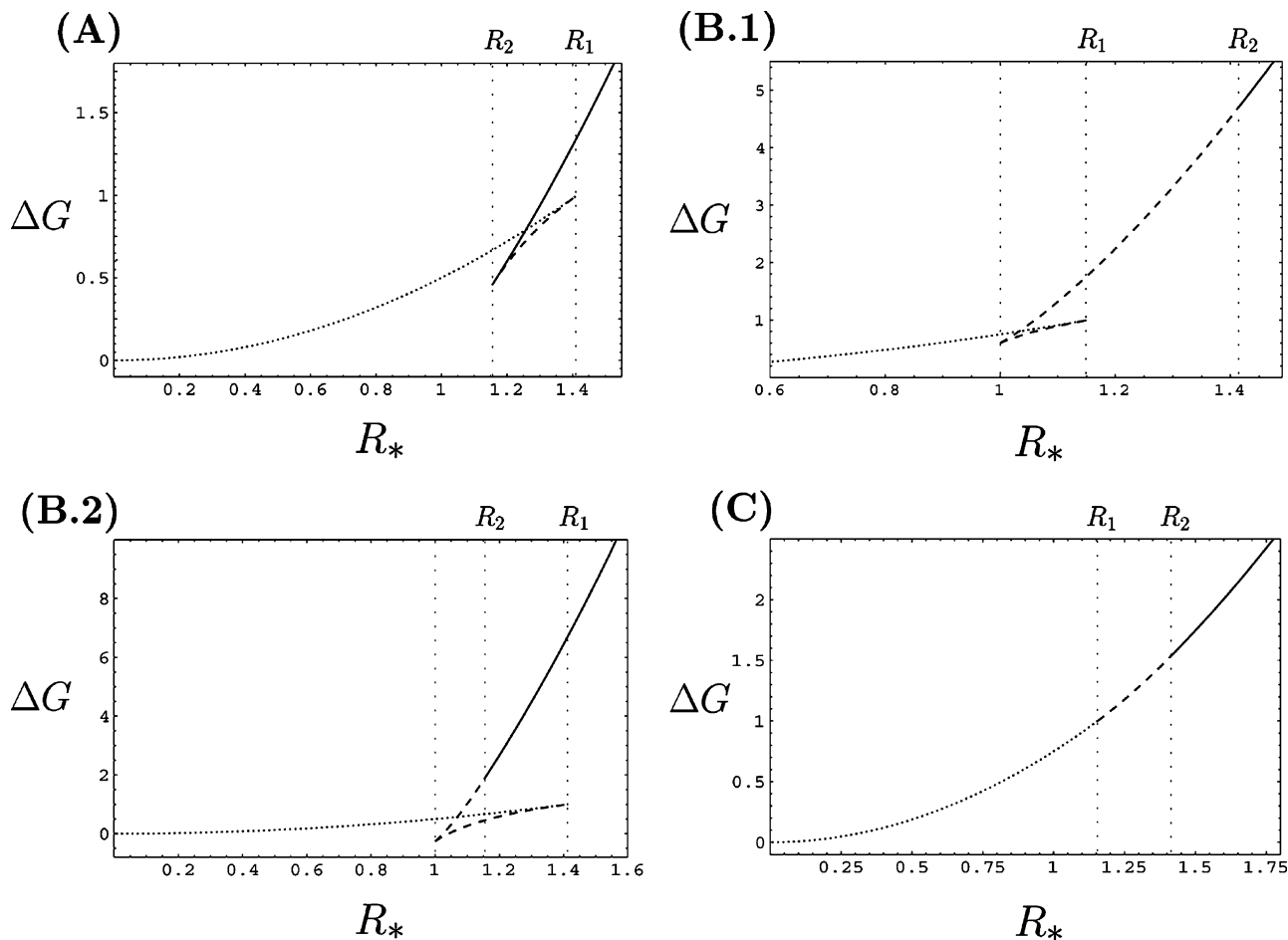


Figure 5. Excess free energy ΔG versus stationary droplet radius R_* for the four parameter regimes (A–C) with the same contact angles as in Figure 3. The stationary radius R_* is given in units of the radius r_γ of the lyophilic circular domain, and ΔG is normalized to its value for $R_* = R_1$. In each case, the dotted curve corresponds to regime I, the dashed curve to regime II, and the solid curve to regime III.

monomers directly with other droplets but only with the vapor phase.

It has been previously shown that, in chemical (or monomer exchange) equilibrium between droplets, the pattern of droplets that forms at a lyophobic surface with N lyophilic circular domains undergoes morphological wetting transitions when the total volume of liquid V_β is changed.¹¹ These transitions are governed by the interfacial free energy ΔF_N of all N droplets that are in monomer exchange equilibrium. In the limit of small contact angle θ_γ , two types of stable droplet patterns are possible: (i) all domains are covered by small droplets of the same size and (ii) one domain is covered by a large droplet, whereas the remaining $N - 1$ domains are covered by small droplets that have, however, the same curvature as the large one. The latter pattern is N -fold degenerate because the large droplet can be located on any of the N lyophilic domains.

If such a droplet pattern is in contact with a super-saturated vapor, its excess free energy is given by

$$\Delta G_N = \Delta F_N - \Delta\mu\rho_\beta\bar{V}_\beta \quad (25)$$

where \bar{V}_β is the total volume of the condensed liquid. This relation represents an obvious generalization of the excess free energy (eq 12) for a single lyophilic domain. Indeed, both free energies correspond to a family of interfacial configurations that have a constant mean curvature $M = 1/R$ and are parametrized by the volume of liquid. These configurations should represent the typical states

of the system provided the domain number N is sufficiently small and the exchange of monomers between these domains is sufficiently fast.

In the following, we will consider the limit of large N and ensembles of droplets that can have any curvature radius R and, thus, any mean curvature M . The volume V_β of a single droplet or cluster can be expressed in terms of the number of monomers n that have joined to form it, via

$$V_\beta = n/\rho_\beta \quad (26)$$

where ρ_β is the particle number density in the β phase. We will assume that the liquid phase is incompressible, which implies that $\rho_\beta = \text{constant}$. Therefore, the monomer number n also provides a convenient measure of the size of the droplets or clusters.

Consider a state in which the system may contain droplets of any size. Let us denote with f_n the number of droplets of size n . The excess free energy of the whole system, $\Delta\mathcal{G}_N$, between this state and a reference state at the same temperature and pressure that contains only vapor and no droplets is

$$\Delta\mathcal{G}_N = \sum_n f_n \Delta G_n - T \ln \Omega \quad (27)$$

where ΔG_n is the excess free energy in the formation of a droplet of size n on a single lyophilic domain (see section

2) and $\ln \Omega$ is the entropy of mixing (as before, the Boltzmann constant k_B has been absorbed into T). The number of possible configurations that arise from distributing the clusters among the N lyophilic domains is $\Omega = N! / [(N - \sum_i f_i)! \prod_j f_j!]$, where the total number of clusters $\sum_i f_i$ is smaller or equal to N . Using Stirling's formula as given by $\ln n! \approx n \ln n - n$, one obtains

$$\ln \Omega \approx -(N - \sum_i f_i) \ln \frac{N - \sum_i f_i}{N} - \sum_i f_i \ln \frac{f_i}{N} \quad (28)$$

In equilibrium with $\Delta\mu \leq 0$, one has

$$\partial \Delta \mathcal{G}_N / \partial f_n = 0 \quad \text{for} \quad f_n = f_n^{\text{eq}} \quad (29)$$

which leads to

$$f_n^{\text{eq}} = (N - \sum_i f_i^{\text{eq}}) \exp(-\Delta G_i / T) \quad (30)$$

Summing eq 30 for all sizes n , one has that at equilibrium the total number of droplets in the whole system $\sum_i f_i^{\text{eq}}$ is

$$\sum_i f_i^{\text{eq}} = N \frac{\sum_i \exp(-\Delta G_i / T)}{1 + \sum_i \exp(-\Delta G_i / T)} < N \quad (31)$$

Inserting this expression into eq 30, one finally arrives at

$$f_n^{\text{eq}} = N \frac{\exp(-\Delta G_n / T)}{1 + \sum_i \exp(-\Delta G_i / T)} \quad (32)$$

This distribution will now be supplemented by two boundary values, n_l and n_r , for the cluster size n . The second value n_r is necessary to analytically continue expression 32 for the cluster size distribution to $\Delta\mu > 0$.

First, let us call n_l the size of the smallest cluster that can be distinguished from homophase (vaporlike) fluctuations of the vapor phase.²⁴ By definition, a cluster of size n_l may break into n_l monomers and dissolve in the vapor phase.

In addition to the lower bound $n = n_l$ for the cluster size, we must also introduce an upper bound $n = n_r$ (where the subscript r stands for "right boundary condition"). For an undersaturated or saturated vapor with $\Delta\mu \leq 0$, the expression as given by eq 32 yields the equilibrium distribution of the droplet sizes. But, for a supersaturated vapor with $\Delta\mu > 0$, the excess free energy ΔG_n behaves as $\sim -\Delta\mu n$ and $\exp(-\Delta G_n / T)$ diverges for large n . Therefore, the sum in the denominator of eq 32 is infinite and $f_n^{\text{eq}} \approx 0$ for all n , which means that the droplets grow to infinite size and the system fills with liquid unless the values of n are restricted to $n \leq n_r$.

In classical nucleation theory, one assumes that for $\Delta\mu > 0$ the distribution f_n^{eq} as given by eq 32 but restricted to the cluster size range $n_l \leq n \leq n_r$ corresponds to a "quasi-equilibrium" characterized by vanishing flux in the cluster

size space as will be explained in the next section. Therefore, we will denote this *zero-flux distribution* by

$$f_n^0 = N \frac{\exp(-\Delta G_n / T)}{1 + \sum'_i \exp(-\Delta G_i / T)} \quad \text{for} \quad n_l \leq n \leq n_r \quad (33)$$

where the prime indicates that the summation over i is also restricted to $n_l \leq i \leq n_r$. If the total number of droplets as given by $\sum'_n f_n^0$ is small compared to the number of domains N , one has $\sum'_n \exp(-\Delta G_n / T) \ll 1$, and the zero-flux distribution is given by the simple expression

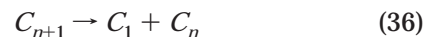
$$f_n^0 \approx N \exp(-\Delta G_n / T) \quad \text{for} \quad n_l \leq n \leq n_r \quad (34)$$

4. Equations of the Kinetics

4.1. Master Equations. Let us assume that the clusters grow (shrink) via the attachment (detachment) of single monomers. On one hand, the growth of the clusters is governed by elementary reactions, consisting of the combination of a single monomer C_1 with a cluster C_n to form a cluster C_{n+1} , that is,



On the other hand, the clusters shrink via reactions of the form



corresponding to the evaporative loss of a single monomer. Hence, the clusters of size C_n can disappear either by decaying into C_{n-1} , through the loss of a monomer or by growing into C_{n+1} by the addition of a monomer.

If $f_n(t)$ is the number of clusters of size n at any instant of time t , we may write

$$\frac{d}{dt} f_n(t) = J_{n-1}(t) - J_n(t) \quad (37)$$

where

$$J_n(t) = k_n^+ f_n(t) - k_{n+1}^- f_{n+1}(t) \quad (38)$$

The *attachment rate* k_n^+ is the number of monomers that condense onto a droplet of size n per unit time, and the *detachment rate* k_n^- is the number of monomers that evaporate from such a droplet per unit time. Because we fix the supersaturation, the attachment and detachment rates for a certain cluster of size n do not depend on the time but only on the size of the cluster.

The quantity $J_n(t)$ is the *net* number of clusters of size n that grow to size $n+1$ per unit time. We will call $J_n(t)$ the *flux* of clusters in the cluster size space. The relations 37 and 38 yield the *master equations* of the nucleation process. A pictorial representation of the transitions between clusters of nearest-neighbor sizes is given in Figure 6.

4.2. Transition Rates. If the attachment of monomers to the droplets occurs directly from the vapor, the *attachment rate* k_n^+ follows from the kinetic theory of gases.^{28,29} If the vapor phase α is treated as an ideal gas

(28) Present, R. D. *Kinetic theory of gases*; McGraw-Hill: New York, 1958.

(29) Wu, D. T. *Solid State Phys.* **1997**, *50*, 37–187.

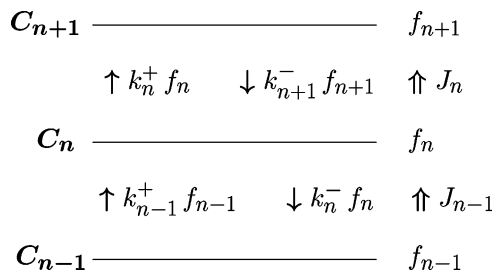


Figure 6. Schematic representation of the transition fluxes J_n and J_{n-1} in cluster size space. The clusters that contain n monomers are denoted by C_n . The quantity f_n is the number of clusters of size n , and the parameters k_n^+ and k_n^- are the attachment and the detachment rates of monomers for a cluster of size n , respectively.

at temperature T and pressure P_α , which contains molecules of mass m_p , this theory leads to

$$k_n^+ = s_n \frac{P_\alpha}{\sqrt{2\pi T m_p}} A_{\alpha\beta} \quad (39)$$

with the interfacial area

$$A_{\alpha\beta} = \left[\frac{36\pi n^2}{\rho_\beta^2 \Phi^2(\theta)} \right]^{1/3} \frac{1 - \cos \theta}{2} \quad (40)$$

of the $\alpha\beta$ interface. The quantities ρ_β , n , and θ are the particle number density in the β phase, the number of monomers condensed to form the droplet, and the actual contact angle of the droplet, respectively. The function $\Phi(\theta)$ has been defined in eq 3. The first factor s_n on the right-hand side of eq 39 is the sticking coefficient, with $0 < s_n < 1$, which corresponds to the probability that a monomer, which collides with the n droplet, actually sticks to it. The quantity $P_\alpha/(2\pi T m_p)^{1/2}$ is the Hertz–Knudsen impingement rate of monomers onto a planar interface per unit area.

Note that eq 39 is valid in any of the regimes (I, II, and III) that we have distinguished for a droplet on a lyophilic circular domain; see section 2.

For simplicity, we have assumed in eq 39 that all the monomers that attach to the droplets come directly from the vapor. It may also happen that most of the monomers that condense onto the droplets are previously adsorbed on the substrate and that the droplets grow by surface migration of these monomers to the three-phase contact line (or by a combination of monomers previously adsorbed on the substrate and monomers coming directly from the vapor). In this more general case, one would have to use a different functional form to evaluate k_n^+ , but the theory presented in this article would still apply.

The detachment rate k_n^- is determined by the thermally activated process of breaking the bonds that bind a monomer to the rest of the cluster. Because there are no simple expressions for the detachment rate, classical nucleation theory relies on an artificial *constrained equilibrium hypothesis* to estimate it. As explained in the previous section, we imagine that a constraint is imposed on the system such that there are no clusters with size $n > n_r$. The system is then described by the zero-flux distribution f_n^0 as given by eq 34. When this distribution is inserted into eq 38, one obtains

$$0 = k_n^+ f_n^0 - k_{n+1}^- f_{n+1}^0 \quad (41)$$

or the detachment rate

$$k_{n+1}^- = (f_n^0/f_{n+1}^0)k_n^+ \quad (42)$$

5. Steady-State Nucleation

Let us consider a steady state in which the size distribution of the clusters does not change with time t . We denote such a steady-state cluster size distribution by f_n^s . In an experiment, the steady state is the plateau region reached after a transient time in which the system “forgets” the initial conditions and before the number of lyophilic domains, where nucleation can still occur, has been significantly reduced.

Because the cluster size distribution does not change with time in the steady state, the relations 37 and 38 imply that the fluxes are time-independent and are equal for all cluster sizes, that is, $J_n = \mathcal{J}^s$ for all n , where \mathcal{J}^s is the steady-state flux. If the steady-state values for the flux and the size distribution are inserted into eq 38, one obtains

$$\mathcal{J}^s = k_n^+ f_n^s - k_{n+1}^- f_{n+1}^s \quad (43)$$

We will impose now the usual boundary conditions of classical nucleation theory:

(i) Let us assume that the clusters of size $n \geq n_r$ are removed from the system, broken up into monomers, and added again to the system, so that the total number of monomers is constant. As mentioned, the subscript r stands for “right boundary condition”. This condition may be implemented in our formalism by the definition

$$f_n^s = 0 \quad \text{for } n \geq n_r \quad (44)$$

However, we will also assume that the zero-flux distribution for $n = n_r$ is still given by eq 34.

(ii) For small clusters, f_n^0 and f_n^s are very large in comparison with their values at the maxima of the double barrier. Thus, it is reasonable to use the boundary condition

$$f_n^s = f_n^0 \quad \text{for } n \leq n_l \quad (45)$$

where l stands for “left boundary condition”. As mentioned, n_l corresponds to the smallest cluster that can be distinguished from homophase fluctuations of the vapor phase.

The first and second maximum of the free energy barrier are located at $n \equiv n_a$ and $n \equiv n_c$, respectively. As long as $n_l \ll n_a$ and $n_r \gg n_c$, the nucleation rates should be insensitive to the actual values of n_l and n_r .³⁰

5.1. Discrete Model for Steady-State Nucleation. It follows from eqs 42 and 43 that the steady-state flux \mathcal{J}^s satisfies the relation

$$\frac{\mathcal{J}^s}{k_n^+ f_n^0} = \frac{f_n^s}{f_n^0} - \frac{f_{n+1}^s}{f_{n+1}^0} \quad (46)$$

Summing the left- and right-hand sides of eq 46 from n_l

(30) Kelton, K. F.; Greer, A. L.; Thompson, C. V. *J. Chem. Phys.* **1983**, *79*, 6261–6276.

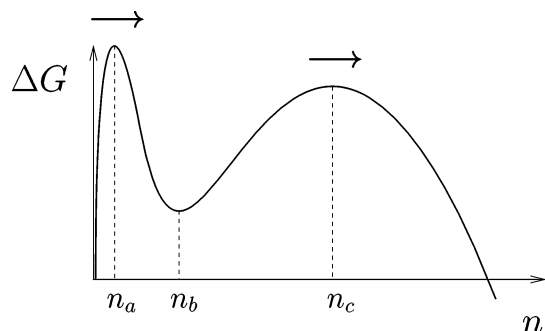


Figure 7. Excess free energy ΔG as a function of monomer number or cluster size n for nucleation through a double barrier. The two arrows correspond to the two fluxes $J(n_a, t)$ and $J(n_c, t)$ in cluster size space as discussed in the text.

to $n_r - 1$ and applying the boundary conditions as given by eqs 44 and 45, one obtains the equation

$$J^s = \left(\sum_{n=n_a}^{n_r-1} \frac{1}{k_n^+ f_n^0} \right)^{-1} \quad (47)$$

by which the steady-state flux J^s is expressed in terms of the zero-flux distribution f_n^0 and the attachment rates k_n^+ .

Likewise, if we sum eq 46 from n to $n_r - 1$ we obtain the expression

$$f_n^s = J^s f_n^0 \sum_{i=n}^{n_r-1} \frac{1}{k_i^+ f_i^0} \quad (48)$$

for the steady-state distribution, where J^s is given by eq 47.

5.2. Continuum Model for Steady-State Nucleation. *5.2.1. Flux in the Steady State.* Let us now assume that n can be treated as a continuous variable. In this continuum limit, the sum in eq 47 is replaced by an integral and we obtain

$$J^s = \left[\int_{n_a}^{n_r} \frac{dn}{k^+(n) f^0(n)} \right]^{-1} \quad (49)$$

If nucleation occurs through a double free energy barrier, it is convenient to divide the integral in eq 49 into two parts, one for each of the maxima. If n_a and n_c are the values of n corresponding to the first and second maxima, respectively, and n_b is the value corresponding to the minimum between these maxima (compare Figure 7), the steady-state flux is given by

$$J^s = \left[\int_{n_a}^{n_b} \frac{dn}{k^+(n) f^0(n)} + \int_{n_b}^{n_r} \frac{dn}{k^+(n) f^0(n)} \right]^{-1} \quad (50)$$

In this expression, the main contributions to the integrals come from the vicinities of the maxima of $\Delta G(n)$. Let us approximate $\Delta G(n)$ in the neighborhood of $n = n_a$ by its Taylor expansion truncated to second order. Because $n = n_a$ corresponds to a maximum, $\Delta G'(n_a) = 0$ and $\Delta G''(n_a) < 0$. Inserting this truncated expansion in $f^0(n)$, one obtains the saddle-point approximation

$$f^0(n) \approx f^0(n_a) \exp[Z_a^2 \pi (n - n_a)^2] \quad (51)$$

with the so-called *Zeldovich factor*

$$Z_a \equiv \sqrt{|\Delta G''(n_a)|/2\pi T} \quad (52)$$

The same saddle-point approximation close to the second maximum leads to

$$f^0(n) \approx f^0(n_c) \exp[Z_c^2 \pi (n - n_c)^2] \quad (53)$$

with the second Zeldovich factor

$$Z_c \equiv \sqrt{|\Delta G''(n_c)|/2\pi T} \quad (54)$$

Now we can approximate $f^0(n)$ by eq 51 in the first integral of eq 50 and by eq 53 in the second integral of eq 50.

Compared to $f^0(n)$, the attachment rate $k^+(n)$ is a slowly varying function of n , because $k^+(n) \sim n^{2/3}$ from eqs 39 and 40. Thus, one can approximate $k^+(n)$ by its value at the first maximum $k^+(n_a)$ in the first integral of eq 50 and by its value at the second maximum $k^+(n_c)$ in the second integral.

Because the main contributions to the integrals in eq 50 come from the vicinities of the maxima of $\Delta G(n)$, the values of these integrals do not change appreciably if one extends their upper limits to infinity and their lower limits to minus infinity. After these approximations in eq 50, the integrals that are left are of the type $\int_{-\infty}^{\infty} \exp(-ax^2) dx = (\pi/a)^{1/2}$, with $a > 0$. In this way, one obtains

$$J^s \approx \left[\frac{1}{k^+(n_a) f^0(n_a) Z_a} + \frac{1}{k^+(n_c) f^0(n_c) Z_c} \right]^{-1} \quad (55)$$

for the steady-state flux through a double free energy barrier.

If one repeats the last calculation for a barrier with only one of the maxima of the double barrier, say the one at $n = n_a$, one finds that the flux in the steady state is $k^+(n_a) f_{a1}^0(n_a) Z_a$. If one has only the maximum at $n = n_c$, the flux in the steady state is $k^+(n_c) f_{c1}^0(n_c) Z_c$. The functions $f_{a1}^0(n)$ and $f_{c1}^0(n)$ are the zero-flux distributions if there is only the first maximum and only the second maximum of the double barrier, respectively. Thus, we may define the two fluxes

$$J_{a1}^s \equiv k^+(n_a) f_{a1}^0(n_a) Z_a \quad \text{and} \quad J_{c1}^s \equiv k^+(n_c) f_{c1}^0(n_c) Z_c \quad (56)$$

which are the classical results for the nucleation through a barrier with a single maximum.³¹

With the help of eq 56, relation 55 can be written as

$$\frac{1}{J^s} \approx \frac{1}{J_{a1}^s} + \frac{1}{J_{c1}^s} \quad (57)$$

Thus, the inverse steady-state flux through a double barrier is equal to the sum of the inverse steady-state fluxes through two barriers with a single maximum. Because these fluxes are positive quantities, it follows from eq 57 that the steady-state flux through a double barrier J^s is smaller than both J_{a1}^s and J_{c1}^s .

Notice that the depth of the minimum between the maxima of the double barrier did not enter our result for J^s . As shown elsewhere, this depth is relevant for the time evolution during the early stage of the nucleation process, that is, before the system reaches the steady state. One of us has solved the corresponding problem of transient nucleation,³² from which one recovers the steady-state

(31) McDonald, J. E. *Am. J. Phys.* **1963**, *31*, 31–41.

(32) Valencia, A. Manuscript to be submitted for publication.

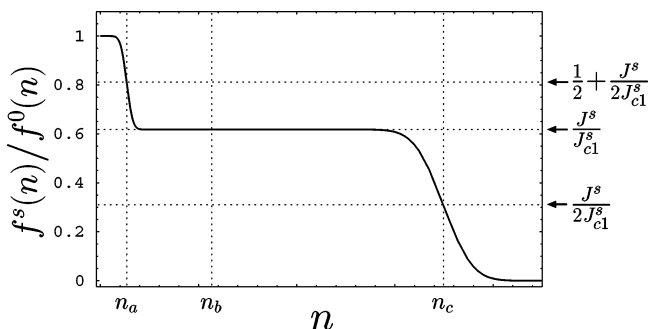


Figure 8. Example for the steady-state distribution f^s divided by the zero-flux distribution f^0 as a function of the monomer number or cluster size n for nucleation through a double barrier as given by eqs 59 or 63. The cluster sizes n_a and n_c correspond to the maxima of the excess free energy $\Delta G = \Delta G(n)$, and the cluster size n_b corresponds to the minimum between these maxima; see Figure 7.

solution (eq 57) for long times, which confirms that the steady-state flux J^s does not depend on the depth of the minimum between the maxima.

5.2.2. Cluster Size Distribution in the Steady State. The steady-state distribution can be obtained from eq 48. In the continuous limit, one has

$$f^s(n) = J^s f^0(n) \int_n^{n_c} \frac{dm}{k^+(m) f^0(m)} \quad (58)$$

where J^s is the steady-state flux that we have already computed.

Using the same saddle-point approximations as those in the previous subsection, one obtains

$$\frac{f^s(n)}{f^0(n)} \approx \frac{J^s}{2} \left\{ \frac{\operatorname{erfc}[Z_a \sqrt{\pi}(n - n_a)]}{k^+(n_a) f^0(n_a) Z_a} + \frac{\operatorname{erfc}[Z_c \sqrt{\pi}(n - n_c)]}{k^+(n_c) f^0(n_c) Z_c} \right\} \quad (59)$$

where Z_a and Z_c are given by eqs 52 and 54, respectively, and $\operatorname{erfc}(x)$ denotes the complementary error function defined by³³

$$\operatorname{erfc}(x) \equiv \frac{2}{\sqrt{\pi}} \int_x^{\infty} \exp(-u^2) du \quad (60)$$

The functional dependence of f^s/f^0 on n is schematically shown in Figure 8.

Let us call $f_{a1}^s(n)$ and $f_{c1}^s(n)$ the steady-state distributions for those cases in which there is *only* the first maximum and *only* the second maximum of the double barrier, respectively. Using the same approximations as before and relations 56 for the corresponding fluxes, we obtain

$$\frac{f_{a1}^s(n)}{f_{a1}^0(n)} \approx \frac{1}{2} \operatorname{erfc}[Z_a \sqrt{\pi}(n - n_a)] \quad (61)$$

and

$$\frac{f_{c1}^s(n)}{f_{c1}^0(n)} \approx \frac{1}{2} \operatorname{erfc}[Z_c \sqrt{\pi}(n - n_c)] \quad (62)$$

If one uses expression 34 for the zero-flux distribution, one obtains $f_{a1}^0(n_a) = f^0(n_a)$ and $f_{c1}^0(n_c) = f^0(n_c)$ at the maxima of the double barrier, which implies

$$\frac{f^s(n)}{f^0(n)} \approx \frac{J^s}{J_{a1}^s} \frac{f_{a1}^s(n)}{f_{a1}^0(n)} + \frac{J^s}{J_{c1}^s} \frac{f_{c1}^s(n)}{f_{c1}^0(n)} \quad (63)$$

as follows from a combination of eqs 56, 59, 61, and 62.

If expression 63 is evaluated at $n = n_a$ and $n = n_c$, the relation $\operatorname{erfc}(0) = 1$ together with the asymptotic behavior $\operatorname{erfc}(x) \approx 0$ for large positive x and $\operatorname{erfc}(x) \approx 2$ for large negative x lead to

$$\frac{f^s(n_a)}{f^0(n_a)} \approx \frac{1}{2} + \frac{J^s}{2J_{c1}^s} = 1 - \frac{J^s}{2J_{a1}^s} \quad (64)$$

and

$$\frac{f^s(n_c)}{f^0(n_c)} \approx \frac{J^s}{2J_{c1}^s} \quad (65)$$

where we have also employed relation 57 between the different fluxes.

From eqs 61 and 62, one has $f_{a1}^s(n) \approx 0$ and $f_{c1}^s(n)/f_{c1}^0(n) \approx 1$ for $n_a \ll n \ll n_c$. Using these approximations in eq 63, one obtains

$$\frac{f^s(n)}{f^0(n)} \approx \frac{J^s}{J_{c1}^s} \quad \text{for } n_a \ll n \ll n_c \quad (66)$$

6. Summary and Outlook

In summary, depending on the values of the supersaturation and of the contact angles, θ_γ and θ_δ , in the lyophilic and in the lyophobic surface domains, the free energy barrier for the nucleation of a droplet on a lyophilic circular domain can have a single maximum or two maxima (a double barrier). The existence of a double barrier is possible because of the nonmonotonic variation of the radius of curvature R of the vapor–liquid interface with the volume V_β of the droplet.

We have shown that surface nucleation through a double barrier occurs for *intermediate* values of the supersaturation. It is convenient to describe this regime in terms of the dimensionless supersaturation Δ as defined by eq 21. To have a double barrier for a circular surface domain, this supersaturation must satisfy inequalities 22 or 23, which correspond to (i) $\sin \theta_\gamma < \Delta < \sin \theta_\delta$ for $\theta_\gamma < \theta_\delta < \pi/2$, that is, when both contact angles are smaller than 90° , or (ii) $\sin \theta_\gamma < \Delta < 1$ for $\theta_\gamma < \pi/2 < \theta_\delta$, that is, when θ_γ is smaller and θ_δ is larger than 90° . No double barrier is possible, on the other hand, if both contact angles exceed 90° .

Thus, the largest range of supersaturations for which surface nucleation at a lyophilic domain proceeds through a double barrier is found in the limit of *small* θ_γ . In this limit, the small supersaturation regime, which extends over the range $0 < \Delta < \sin \theta_\gamma$ and which is characterized by a single barrier, shrinks to 0. In such a case, for $\theta_\delta > \pi/2$ one has a double barrier if the dimensionless supersaturation Δ satisfies $0 < \Delta < 1$. In terms of the physical, dimensional quantities, these inequalities are equivalent to $0 < \Delta\mu < 2\Sigma_{\alpha\beta}/\rho_\beta r_\gamma$.

For a supersaturated vapor, one has $\Delta\mu \approx T \ln(P_\alpha/P_0)$ as given by eq 20, which implies $\Delta\mu \approx T(P_\alpha - P_0)/P_0$ if the vapor pressure P_α is close to the saturation pressure P_0 .

(33) Spiegel, M. R.; Liu, J. M. *Mathematical handbook of formulas and tables*; McGraw-Hill: New York, 1998.

Therefore, for contact angles $\theta_\gamma = 0$ and $\theta_\delta > \pi/2$, surface nucleation proceeds through a double barrier if the pressure difference satisfies $0 < (P_\alpha - P_0)/P_0 < 2\Sigma_{\alpha\beta}/T\rho_\beta r_\gamma$.

As an example, let us consider the condensation of water at room temperature with interfacial tension $\Sigma_{\alpha\beta} \approx 72$ mJ/m² and particle number density $\rho_\beta \approx 30/\text{nm}^3$. The size r_γ of the lyophilic surface domain is taken to be $r_\gamma \equiv \bar{r}$ nm. One then arrives at the inequalities $0 < (P_\alpha - P_0)/P_0 < 1.2/\bar{r}$ for surface nucleation with a double barrier. For relatively small surface domains with $1 \lesssim \bar{r} \lesssim 10$, such pressure differences should be experimentally accessible. (For small domain sizes in the nanometer regime, the line tension of the contact line will also contribute to the excess free energy. It is not difficult to incorporate these contributions into the theory presented here.) For relatively large surface domains with $r_\gamma > 1$ μm or $\bar{r} > 10^3$, on the other hand, the experimental pressure control of $(P_\alpha - P_0)/P_0$ must be better than $1/10^3$ to access the double barrier regime.

We have also solved the problem of the kinetics of nucleation through a double barrier on N lyophilic circular domains. We derived expressions for the flux and the cluster size distribution in the steady state. Most remarkably, these quantities can be written as simple combinations of the classical results for nucleation through a barrier with a single maximum; see eqs 57 and 63.

In particular, we found that the inverse steady-state flux through a double barrier is equal to the sum of the inverse steady-state fluxes through two barriers with a single maximum; see eq 57. Notice that the flux at the steady state does not depend on the depth of the minimum between the maxima. This result is confirmed by the solution for the time evolution of nucleation in the transient regime (i.e., the regime before the steady state is established), as will be discussed elsewhere.³²

Acknowledgment. One of the authors, A.V., would like to thank Stefan Klumpp and Haijun Zhou for fruitful discussions. This work was partially supported by the Deutscher Akademischer Austausch Dienst.

List of Symbols

α	vapor phase
β	liquid phase
γ	lyophilic surface domain
Δ	reduced supersaturation
δ	lyophobic surface domain
θ	actual contact angle of the droplet
$\theta_\gamma, \theta_\delta$	contact angle on a γ and δ domain
μ_α, μ_β	chemical potential in the α and β phase
$\Delta\mu$	supersaturation
ρ_α, ρ_β	particle number density in the α and β phase
Σ_{ij}	surface tension of the ij interface
$\Phi(\theta)$	wetting function
Ω	number of complexions of the droplets on N lyophilic circular domains

A_{ij}	surface area of the ij interface
C_n	cluster of size n
ΔF	excess interfacial free energy
ΔF_N	ΔF for N lyophilic domains
$f_n(t)$	discrete cluster size distribution at time t
$f(n, t)$	continuous cluster size distribution at time t
$f^{\text{eq}}(n)$	equilibrium cluster size distribution
$f^0(n)$	zero-flux distribution
$f_{a1}^0(n)$	zero-flux distribution if only first maximum
$f_{c1}^0(n)$	zero-flux distribution if only second maximum
$f^s(n)$	steady-state distribution
$f_{a1}^s(n)$	steady-state distribution if only first maximum
$f_{c1}^s(n)$	steady-state distribution if only second maximum
ΔG	excess Gibbs free energy for one lyophilic domain
ΔG_N	excess Gibbs free energy for N domains (without the mixing entropy)
$\Delta \mathcal{G}_N$	excess Gibbs free energy for N domains (with the mixing entropy)
$J(n, t)$	flux of clusters in the size space
\mathcal{J}	steady-state flux
J_{a1}^s, J_{c1}^s	flux in the steady state if <i>only</i> one of the maxima of the double barrier exists
k_B	Boltzmann's constant
k_n^+, k_n^-	monomer attachment and detachment rate
M	mean curvature
m_p	mass of a monomer
N	number of lyophilic circular domains
n	number of monomers in a cluster
n_a, n_c	first and second maxima of $\Delta G(n)$
n_b	minimum between the maxima of $\Delta G(n)$
n_l	smallest cluster size
n_r	largest cluster size
P	pressure
P_0	saturated vapor pressure
P_α, P_β	pressure in the α and β phase
R	radius of curvature of the α - β interface
R_*	stationary radius of curvature
R_1	R of a droplet of volume V_1
R_2	R of a droplet of volume V_2
r_γ	radius of the lyophilic circular domains
s_n	sticking coefficient of the attachment rate
T	temperature
t	time
V_β	volume of one droplet
\bar{V}_β	volume of liquid in the whole system
V_1	smallest volume of a droplet in regime II
V_2	largest volume of a droplet in regime II
V_{sp}	volume of the sphere with radius r_γ
Z_a, Z_c	Zeldovich factors at the maxima of $\Delta G(n)$

LA0354741